AFRL-OSR-VA-TR-2014-0055

Low Noise Mid-Wavelength IR Photodetectors

RUI YANG

UNIV OF OKLAHOMA

02/19/2014
Final Report

AIR FORCE RESEARCH LABORATORY
AF OFFICE OF SCIENTIFIC RESEARCH (AFOSR)/RSE
ARLINGTON, VIRGINIA 22203
AIR FORCE MATERIEL COMMAND

REPORT DOCUMENTATION PAGE

Form Approved
OMB No. 0704-0188

1. REPORT DATE *(DD-MM-YYYY)*	**2. REPORT TYPE**	**3. DATES COVERED** *(From - To)*
02-16-2014	Final Performance Report	June 2012 – Nov. 2013

4. TITLE AND SUBTITLE

Low Noise Mid-Wavelength IR Photodetectors

5a. CONTRACT NUMBER
FA9550-12-1-0260

5b. GRANT NUMBER

5c. PROGRAM ELEMENT NUMBER
AFOSR

6. AUTHOR(S)
Rui Q. Yang

5d. PROJECT NUMBER
120230

5e. TASK NUMBER

5f. WORK UNIT NUMBER

7. PERFORMING ORGANIZATION NAME(S) AND ADDRESS(ES)

University of Oklahoma
110 West Boyd Street
Norman, OK 73019

8. PERFORMING ORGANIZATION REPORT NUMBER

AFOSR-002FPR

9. SPONSORING / MONITORING AGENCY NAME(S) AND ADDRESS(ES)

Air Force Office of Scientific Research
Dr. Kitt Reinhardt (to 9/30/2012) and Dr. James C. M. Hwang
875 N. Randolph Street
Arlington, VA 22203

10. SPONSOR/MONITOR'S ACRONYM(S)
AFOSR

11. SPONSOR/MONITOR'S REPORT NUMBER(S)

12. DISTRIBUTION / AVAILABILITY STATEMENT

Distribution is unlimited

13. SUPPLEMENTARY NOTES

14. ABSTRACT

This report documents the investigations and development of low noise mid-wavelength infrared photodetectors at the University of Oklahoma for a period of time from June 2012 to Nov. 2013. Our technical approach is based on interband cascade IR photodetectors (ICIPs) that are composed of discrete superlattice (SL) absorbers. We developed a unified theory on carrier transport and noise in discrete multiple stage absorber structures and applied the theory to have evaluated the fundamental limit of device performance in terms of the product of absorption coefficient and minority carrier diffusion length. We demonstrated in theory that ICIP device performance can be better in terms of detectivity compared to conventional single-absorber detectors, which is especially significant at high temperatures when the diffusion length is reduced or for high-speed applications. Several ICIP structures were grown by MBE and fabricated into devices with a cut-off wavelength near 4-5 μm. Experimental results obtained from these devices have indicated improved device performance at high temperatures with additional stages as projected qualitatively by the theory.

15. SUBJECT TERMS

Semiconductor infrared photodetectors, quantum wells, type-II superlattices, interband cascade structures.

16. SECURITY CLASSIFICATION OF:			**17. LIMITATION OF ABSTRACT**	**18. NUMBER OF PAGES**	**19a. NAME OF RESPONSIBLE PERSON**
a. REPORT	**b. ABSTRACT**	**c. THIS PAGE**	UU	15	Rui Q Yang
					19b. TELEPHONE NUMBER *(include area code)* 405-325-7361

Final Performance Report
For a period from June 2012 to Nov. 2013 on
An AFOSR Project (Award Number: FA9550-12-1-0260)

Low Noise Mid-Wavelength IR Photodetectors

Rui Q. Yang
School of Electrical and Computer Engineering, University of Oklahoma, Norman, OK 73019

February 15, 2014

Program Manager: Dr. James C. M. Hwang (from 10/01/2012)
Dr. Kitt Reinhardt (to 09/30/2012)
Air Force Office of Scientific Research
875 N. Randolph Street, Arlington, VA 22203

Abstract

This report documents the investigations and development of low noise mid-wavelength infrared photodetectors at the University of Oklahoma for a period of time from June 2012 to Nov. 2013. Our technical approach is based on interband cascade IR photodetectors (ICIPs) that are composed of discrete superlattice (SL) absorbers. We developed a unified theory on carrier transport and noise in discrete multiple stage absorber structures and applied the theory to have evaluated the fundamental limit of device performance in terms of the product of absorption coefficient and minority carrier diffusion length. We demonstrated in theory that ICIP device performance can be better in terms of detectivity compared to conventional single-absorber detectors, which is especially significant at high temperatures when the diffusion length is reduced or for high-speed applications. Several ICIP structures were grown by MBE and fabricated into devices with a cut-off wavelength near 4-5 μm. Experimental results obtained from these devices have indicated improved device performance at high temperatures with additional stages as projected qualitatively by the theory.

I. Introduction

This is the final performance report from the University of Oklahoma (OU) for project entitled "Low noise mid-wavelength IR photodetectors". The performance period of this project is from June 2012 to Nov. 2013.

Our objectives are to advance the understanding of quantum-engineered interband cascade (IC) IR photodetector (ICIP) structures, and develop high-performance low noise mid-infrared (IR) detectors based on type-II ICIP structures that are composed of discrete type-II superlattice (SL) absorbers. The project includes development of theory, device design, molecular beam epitaxy (MBE) growth, device fabrication and characterization. Significant progress has been made and was reported in technical conferences and journal articles [1-4], as well as a Ph.D. dissertation by Hinkey [5] who graduated in Dec. 2013 and is now working at Naval Research Laboratory, Washington DC. Below, some details are provided.

II. Theory of Multiple Stage Interband Cascade IR Photodetectors

II.A. Operation Principle of Quantum Engineered ICIPs

Quantum-engineered ICIPs, which was originated from interband cascade lasers [6-8], exploit a discrete absorber architecture to achieve highly efficient detector function based on new principles that combine the advantages of very fast intersubband relaxation, interband tunneling for carrier transport, and relatively slow interband transitions. As illustrated in Fig. 1, an ICIP structure is composed of multiple stages connected in series that take advantage of the broken-gap alignment in type-II quantum well (QW) structures for facilitating carrier transport. As shown in Fig. 1, each stage is divided into three zones based on three different processes: (1) excitation, (2) intraband relaxation, and (3) interband tunneling [9-11]. Figure 1 shows a section of an ICIP structure including three excitation zones (absorbers made of InAs/GaSb SLs (1)) connected with zones for intraband relaxation (2) and interband tunneling (3). Zones (2) and (3) also act as a hole barrier and an electron barrier, respectively, forming a complementary barrier configuration [12]. One cascade stage can be viewed as a double heterostructure unit. To understand the operation of this structure as a detector, we describe the role of each zone associated with a photo-excited electron moving through the structure. In zone (1), photons excite electrons from state E_h in the valence band to state E_e in the conduction band. The electrons then move to the left through intraband relaxation in zone (2), while holes are confined in zones (1) and (3). The transport of electrons to the right is greatly suppressed because state E_e is located within the bandgap of zone (3), consisting of several GaSb/AlSb QWs. Zone (2) is composed of a series of digitally-graded InAs/AlSb QWs that form an energy ladder with discrete energy levels acting as a slide for electrons to move in a preferred direction. That is, the right end of the energy ladder is near the conduction band of the adjoining absorber, while the left end of the profile is near the valence

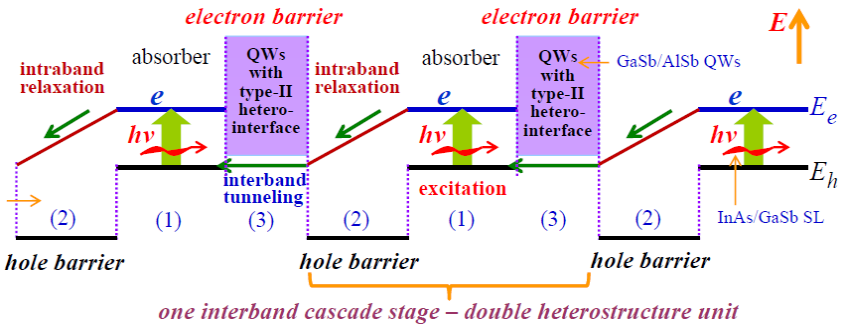

Fig.1. Illustration of operation principle of IC IR photodetector.

band of the absorber adjoining it. After zone (2), electrons return to the valence band state in the adjacent absorber through interband tunneling, facilitated by the type-II band-edge alignment in zone (3). Based on this IC structure, a photocurrent is achieved even without an external bias voltage because of the overall asymmetric band profile of this structure.

Photo-generated carriers can be collected with nearly 100% efficiency because the carriers travel over only a single stage, which is designed to be shorter than a typical diffusion length (estimated to be on the order of ~1 μm). Adding more stages increases photon absorption and reduces noise. Other advantages of this configuration include: reduction of Shockley-Read-Hall recombination current with the elimination of conventional depletion regions in *pn* junctions and the flexibility provided by quantum engineering. For example, ICIPs employ a discrete absorber architecture (similar to QWIPs), where electrons move quickly across a short distance in an individual absorber and are capable of *high-speed* operation without compromising absorption quantum efficiency, while still suppressing noise and maintaining reasonably-high detectivity. The entire ICIP structure can be grown by molecular beam epitaxy (MBE) on an (001) GaSb substrate. With these features, quantum engineered ICIPs provide a most promising option for achieving high performance and high temperature operation.

II.B. Theoretical Framework and Calculated Results

We will first review the theoretical limit for single-stage photovoltaic (PV) detectors and then proceed to the theoretical framework and results for multiple-stage ICIPs.

II.B.1. Finite Collection Limits of Single-Absorber Detectors

A model for treating arbitrary single-absorber PV detectors was presented by Piotrowski and co-workers [13-14]. The detector sensitivity was quantified using the specific detectivity, D^*, given as:

$$D^* = \frac{\lambda}{hc}\frac{\eta}{\sqrt{2(g+r)d}} \quad , \tag{1}$$

where h is Planck's constant, c is the speed of light, η is the detector's external quantum efficiency, d is the detector thickness, and g and r represent the generation and recombination rates in the absorber material. Using this model, they deduced the ultimate performance limits offered by a given infrared detector material. In their treatment, they defined the ultimate performance limit as the performance that was solely limited by the bulk properties of the absorber material. Thus, non-idealities introduced by series resistance, surface generation-recombination effects, and non-ideal contacts are not included in the ultimate limit. It was also assumed that all the carriers generated in the absorber (both photo-generated and thermally generated carriers) are collected and produce charge flowing in the external circuit. This corresponds to an assumption of infinite diffusion length, D_n, (or infinite mobility) in the absorber material.

An important idea presented in Refs. 13 and 14 was the existence of a tradeoff between signal and noise that is faced when designing a detector. This arises from the fact that the photo-generation rate exponentially decays as the light moves deeper into the absorber, while the thermal generation rate is uniform across the absorber. In the limit of $D_n \rightarrow \infty$, the optimal choice for the absorber thickness is $1.26\alpha^{-1}$, where α is the absorption coefficient. This gives an optimized detectivity of:

$$D^* = 0.31 \times k \times \frac{\lambda}{hc}\sqrt{\frac{\alpha}{g}}\,, \tag{2}$$

where for a single-pass of radiation k is a number that varies between 1 and $2^{1/2}$ depending the magnitude of the reverse bias. The value of k equal to unity at zero bias, where r=g, and equal to $2^{1/2}$ under saturation bias where r=0. Note that the reduction in noise (and increased detectivity) with reverse bias application is predicated on the assumption that there is no 1/f noise. However, 1/f noise can often be quite strong in infrared detectors operated in reverse bias, and can limit the amount of noise reduction possible by suppressing the recombination noise component.

Multiple-stage detectors have the potential to achieve better sensitivity than single-absorber detectors in the limit where the carrier collection of the generated carriers in the absorber is limited by a slow diffusion process. Thus, in comparing single- and multiple-stage detectors, it is important to consider how the performance of single-absorber detectors is affected by the speed of the diffusion process in the absorber. When the carrier collection is incomplete, some of the generated carriers will recombine before they are able to contribute to the external signal. Thus, the signal no longer scales with the total generation rate times the absorber thickness, as in Eq. 1, but will scale with the rate of carrier collection. The collection current can be divided into the photo-collection current, G, which arises from the collection of photo-generated carriers, and the thermal collection current, Γ, which arises from the collection of thermally generated carriers. We denote Y as the total collection current, which is the sum of the photo-collection and thermal collection components. The current that arises from application of bias is denoted as the injection current, R. In the limit of $D_n \rightarrow \infty$, the thermal collection current is equal to $g_{th}d$, where g_{th} is the thermal generation rate, and the photo-collection current is equal to the incident photon flux times the external quantum efficiency. Thus, D^* given by Eq. 1 is recovered in this limit. Note that the generation rates are rates per unit volume, while the currents are rates per unit area. The currents are particle currents. The corresponding electrical currents can be obtained by multiplying by the electron charge.

The limiting effects of imperfect carrier collection on the potential performance of a single-absorber detector can be judged by the product of the absorption coefficient, α, and the diffusion length, L_n of the absorber material. The diffusion length is given by $L_n=(D_n\tau)^{1/2}$, where τ is the carrier lifetime in the absorber. A low value of αL_n implies that a single-absorber detector will be unable to convert a large percentage of the incident photon flux to photocurrent, because the total number of electrons excited within a diffusion length of the collection point will be low. This means that even if the absorber is made thick enough to absorb most of the incident photons, many of the photo-excited carriers will recombine before producing signal in the external circuit. When the slow diffusion of carriers becomes a limiting factor in the transport process, both the quantum efficiency and dark current will depend on the carrier diffusion coefficient. The individual collection currents arise from the generation of carriers in the absorber. The reciprocity relations [15-17] can be used to find the probability that a carrier generated at a certain point in the absorber will contribute to the collection current. If the total generation rate at a point x in the absorber is denoted as $g(x)$, and the carrier collection probability at that point is given by f_c(x), the total collection current that flows in the absorber will be given by:

$$Y = \int_0^d dx\, f_c(x) g(x), \tag{3}$$

In obtaining Eq. 3, we have assumed that the absorber extends from x=0 to x=d. Note that Eq. 3 is valid for both thermal (dark) generation and photo-generation. In the subsequent analysis, we consider the case of a flat-band absorber (no electric field) and zero surface recombination velocity across the whole absorber boundary. For this case, the carrier collection probability across the absorber is given by:

$$f_c(x) = \frac{\cosh[(d-x)/L_n]}{\cosh(d/L_n)}, \tag{4}$$

where we denote x=0 as the collection point for the minority carriers.

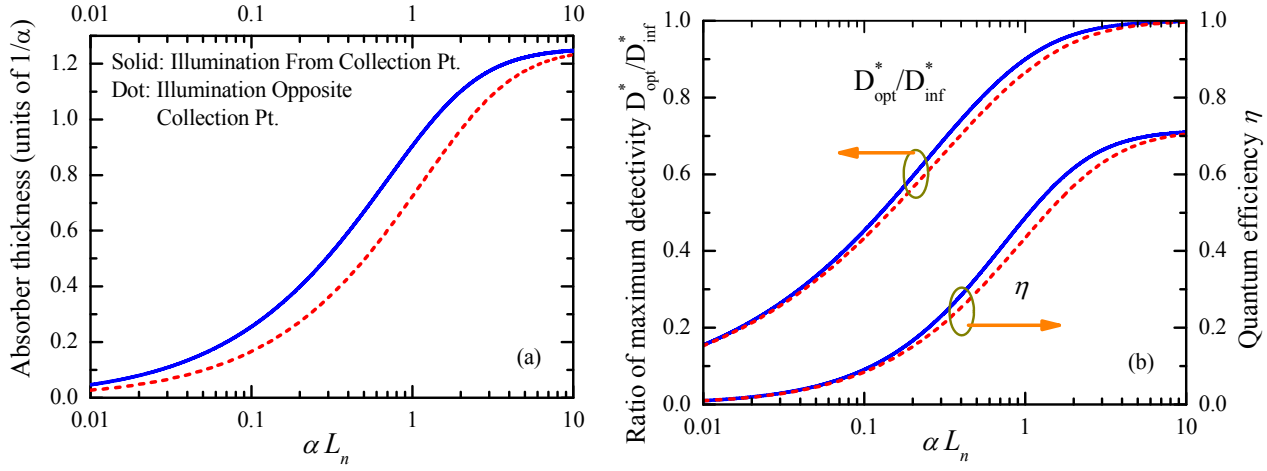

Figure 2. Variation of the performance of optimized single-absorber PV detector as a function of absorber material parameter αL_n. (a) The variation of the optimal absorber thickness in units of absorption depth. (b) The variation of the quantum efficiency and optimal detectivity, D^*_{opt}, for a detector that utilizes the optimal absorber thickness.

From Eq. 3 and Eq. 4, the expressions for the quantum efficiency and the thermal currents can be found for the case of a finite diffusion coefficient [2]. The properties of an optimized detector as a function of αL_n for the case of a flat-band absorber and zero surface recombination velocity are shown in Figure 2. The optimized detector was found by numerically solving for the value of d that maximized D^*. The optimized values of d, given in units of α^{-1}, are shown in Figure 2(a). It can be seen that for lower values of αL_n, the optimal thickness is reduced. The corresponding values of η and D^* are given in Figure 2(b). Note that the D^* values are normalized to the infinite mobility limit value of Eq. 2. For large values of αL_n, the optimal thickness and D^* values approach the values predicted in the infinite mobility limit. However, at lower values αL_n, the limited collection efficiency reduces the detectivity. Results are given for both the situation where the optical signal is incident from the minority collection point (i.e. the photo-generation rate is highest where $f_c(x)$=1), and the situation where light is incident opposite to the minority carrier collection point. Note that the detectivity is higher for the first illumination condition, since more carriers are generated in regions with high collection probabilities.

II.B.2. Improved Carrier Collection in ICIPs

When the absorption and collection process is divided into discrete stages, the individual absorber thicknesses can be kept fairly short. This choice ensures that the most of the photo-generated carriers are collected before they can recombine. The improvement in carrier collection offered by the multiple-stage architecture is illustrated in Figure 3 for detectors with p-type absorbers. This figure compares the absorption and collection process of a single-absorber detector with that of a four-stage detector for the case where $\alpha L_n = 0.5$. The four-stage detector is chosen to have identical stages. The total absorber thickness, d, for both detectors was set equal to the absorption depth. Thus, the absorber thicknesses for the four-stage detector are equal to $d/4$. Since light absorption only occurs in the absorber region, the total absorption efficiency for both detectors is equal. In this example, the light is taken to be incident on the absorber from the minority carrier collection point. The shaded region in the absorber show how the product of the photo-generation rate, $g_{ph}(x)$, and carrier collection probability varies across the absorber region. Following Eq. 4, the product of these two quantities is integrated across each absorber to obtain the photo-collection current in each stage. The total collection efficiency is defined as the percentage of absorbed photons that contribute to the photo-collection current in any of the stages. This collection efficiency is found to be fairly low (54%) for the case of a single-absorber detector. This is because of the low carrier collection probability at points far from the minority carrier collection point. Notably, the carriers that are generated at the right edge of the absorber and have to travel across the entire absorber to be collected only have a collection probability of ~27%. In contrast, each stage in the multiple-stage detector has a carrier collection point at the interface of the hole barrier and the absorber. Since the absorbers are kept short, the collection efficiency stays fairly high across the absorber. This enables the multiple-stage device to achieve a much higher total collection efficiency of 93%. For this case, the carriers generated farthest from the collection point at the right edge of one of the absorbers still have a high collection probability of ~89%.

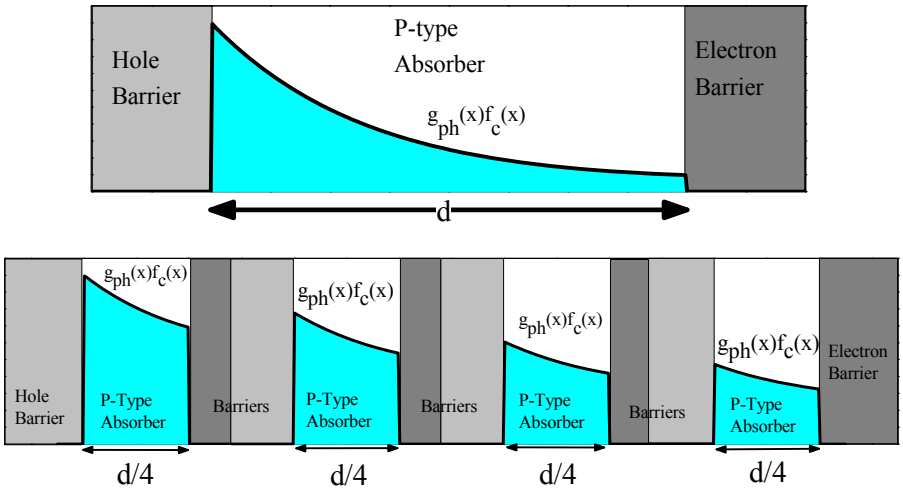

Figure 3. Comparison of collection efficiency in single- and multiple-stage absorbers for detectors using a p-type absorber material with a low αL product.

It should be noted that since infrared detectors are typically operated near zero bias, there is an additional requirement that the device have an equal photocurrent in all stages. This will reduce the effective particle efficiency of the device. In ICIPs the photocurrent will be equal to

the photo-generation rate in the stage with the lowest photo-generation rate. For ICIPs with identical stages, this will be the optically deepest stage. In order to keep a constant current through the device, the other stages must have some compensating injection current. For ICIPs with identical stages, this negates some of the advantages of the multiple-stage architecture. An alternative design choice is to utilize a photocurrent-matched detector design, where the absorber thicknesses are varied across the structure in order to achieve an equal photo-collection current in each stage. It is notable this loss due to the current-matching effects is not present when an illuminated device is operated at zero net current. For an illuminated device with zero current, each photon that contributes to the photo-collection current in any of the stages, requires some additional forward bias to bring the detector to a zero-current condition. This is one reason why the open-circuit voltages in interband cascade structures can be quite high [18].

II.B.3. Noise Reduction in Multiple-Stage Detectors

Even with the improved carrier collection, it may still seem counterintuitive to engineer a photodetector that requires multiple incident photons to generate a single electron in the external circuit. This sort of design probably seems even more ludicrous when it is taken into consideration that an ICIP with several identical stages will have the same saturation dark current as one with a single-stage that is equivalent to those in the multiple-stage device! To truly understand the benefits of a multiple-stage design, it is necessary to consider how the use of multiple stages influences the noise associated with the current flow. For a single-absorber detector, the noise, s_o, can be related to shot noise contributions from the collection and injection currents:

$$s_o = 2e^2 A[Y + R], \tag{5}$$

where e is the electron charge and A is the detector area. The total noise, s_o, is related to the squared noise current by: $i_n^2 = s_o \Delta f$, where Δf is the detector bandwidth. It is sometimes overlooked that Eq. 5 is not a general equation, but only applies in situations where the passage of an electron between the device contacts results from a single type of electron transition event. In standard diffusion-limited PV detectors Eq. 5 normally holds, since the passage of an electron between the contacts relies on a single interband transition. However, in order to pass between the device contacts, a single electron must undergo an interband excitation in each of the N_s absorbers in the device, where N_s denotes the number of stages. The fact that electrons in ICIPs require several transitions in order to traverse through the whole structure means that the noise is reduced below the value predicted in Eq. 5. One can think of the additional interband transitions the electron must undergo as additional trials in an experiment. It is well-known that the uncertainty in experimental measurements can be reduced by adding additional trials. Similarly, in semiconductor devices, the more transitions an electron must undergo as it passes between the contacts of the device, the less noise there will be in the output electrical signal.

A more general expression for the noise can be derived from the Shockley-Ramo theorem. This approach was developed and utilized for calculating the noise in intersubband quantum cascade detectors [19-21]. The Shockley-Ramo theorem gives a connection between the internal device dynamics and the corresponding charge that flows in the external circuit. By applying the Shockley-Ramo theorem, the detector noise can be directly evaluated. This formalism provides a consistent framework for computing both Johnson and shot noise. Applied to ICIPs, the Shockley-Ramo theorem gives the noise as [2]:

$$s_o = 2e^2 A \sum_{m=1}^{N_s} \beta_m^2 (Y_m + R_m), \qquad (6)$$

where Y_m *and* R_m are the individual collection and injection currents in the m^{th} stage, and β_m is the percentage of the total device resistance across the m^{th} stage. The noise reduction in multiple-stage devices can be easily seen by considering the case of an ICIP with identical stages, operating in the thermal-noise limit. In this case, the collection and injection currents are the same in each of the stages, and value of β_m will be equal to $1/N_s$, since the voltage drop will be the same across each of the stages. By setting Y_m=Y and R_m=R, and summing over all the stages, it is found that for ICIPs with identical stages, the total noise, s_o, will be then be equal value given in Eq. 5 divided by a factor of N_s. This implies that the noise current will be reduced by a factor of $N_s^{1/2}$.

II.B.4. Improved Detectivity in Multiple-Stage Detectors

With improvement in carrier collection and noise reduction in ICIPs, the detectivity will be enhanced. We applied our developed theory to two types of multiple-stage detectors. The first design considered is the one where each stage is made to be identical. This type of structure has the advantage of fairly simple design and growth. However, light attenuation limits the output signal current to the value of the photo-collection current in the stage with the lowest photo-collection current. When there is only a single pass of radiation, this will be the optically deepest stage. The second type of structure we consider is one where the absorber thicknesses are varied across the structure in order to achieve an equal photo-collection current in each stage. We refer to this type of design as a photocurrent-matched detector.

There are several possible sources of noise that can influence the sensitivity of infrared sensing systems. The most fundamental source of noise is the inherent fluctuation of either the signal current, or the current induced by the background radiation. This radiative noise will be dominant when the radiative photocurrent J_{rad}, (due to electron photoexcitation from either signal or background radiation) is much higher than the saturation dark current, J_{sat}. In the opposite limit, where J_{sat} >> J_{rad}, the noise is determined by the non-radiative thermal fluctuations of the rate of carrier exchange between the eigenstates of the structure. In addition, there may also be noise introduced by the pre-amplifier and other system components. In this section, we will focus on situation where J_{sat}>>J_{rad}, which is referred to as the thermal noise limit. This is the relevant operation regime for high-temperature sensing applications of relatively weak signals (e.g. photon flux below or comparable

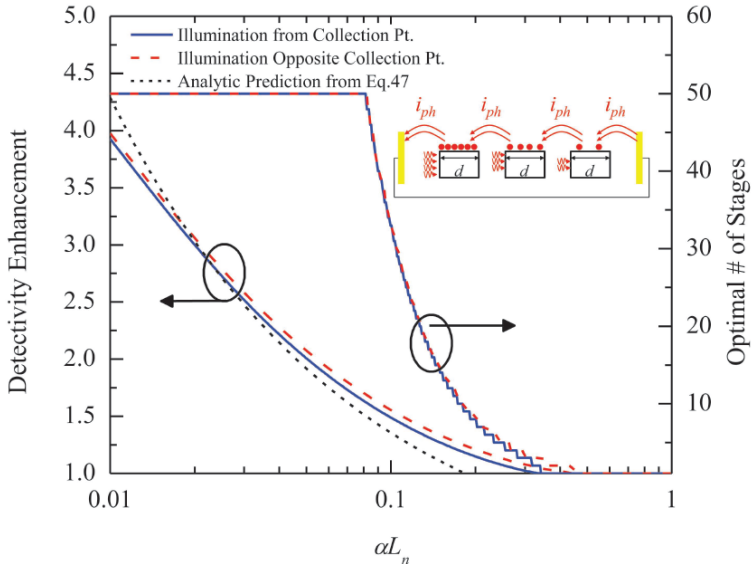

Fig. 4. Theoretical detectivity enhancement for multiple-stage ICIPs with identical stages operating in thermal noise limit as a function of the αL_n.

to that of the background radiation).

For ICIPs with equal-length absorbers, the calculated detectivity enhancement is shown in Fig. 4 [2]. Also shown is the optimal number of stages for the multiple-stage detector as a function of αL_n found from the numerical optimization. From the numerical optimization, it was found that the multiple-stage detector can have superior performance for αL_n less than ~0.4. For very low values of αL_n, the optimal number of stages becomes quite large (e.g. greater than 1000 for $\alpha L_n < 0.02$).

From the results shown in Fig. 4, we see that if we set each absorber to have equal lengths, there will only be appreciable improvements in the sensitivity when the absorber parameter αL_n is less than 0.2. This is because the incident photons are still not used very efficiently, even with the improved collection of absorbed carriers provided by the multiple-stage design. A way to improve the overall particle conversion efficiency is to utilize a "photocurrent-matched" multiple-stage design. In this type of design, the absorber thicknesses are varied throughout the structure so that an equal photo-collection is achieved in each stage when the device is illuminated. Consequently, this approach enables the most efficient usage of the incident photons. The thermal-noise-limited detectivity for photocurrent-matched detectors is given as:

$$D^* = \frac{\lambda}{hc}\frac{\eta_{ext}}{\sqrt{4 g_{th} L_n}}\sqrt{\sum_m \frac{1}{\tanh\left(d_m / L_n\right)}}, \qquad (7)$$

where d_m represents the thickness of the m^{th} absorber. To achieve photocurrent-matching, the d_m are chosen so that the number of collected photocarriers is equal in each stage. The optimized photocurrent-matched detectors were found by identifying the optimal sequence of absorber thicknesses for a detector with a given number of stages. The results are shown in Fig. 5 for 2-stage, 11-stage, and 30-stage detectors with αL_n values ranging from 0.01 to 10. Like the equal-absorber case, it is seen that the advantages of using multiple-stages only become significant when $\alpha L_n < 1$. However, it is interesting to note that there is always a sensitivity advantage to be gained from using multiple stages when operating at zero bias. This result is independent of the material parameters. We can simply illustrate this by comparing a single-stage and two-stage detector in the limit where $L_n \to \infty$, so that: $\eta_{d_m} = 1 - e^{-\alpha d_m}$. For a single-stage device, the optimal absorber thickness that maximizes D^* is d=1.26/α. An optimized two-stage device will have d_1=0.55/α and d_2=1.32/α. The ultimate zero-bias detectivity for this case is then given by:

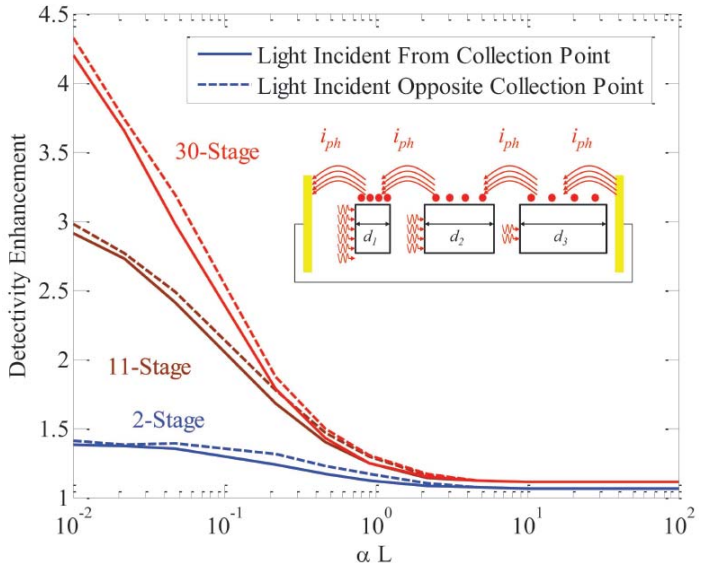

Fig. 5. Theoretical zero-bias detectivity enhancement for 2-stage, 11-stage, and 30-stage photocurrent-matched multiple-stage interband detectors operating the thermal noise limit.

$$D^* = (0.339)\frac{\lambda}{hc}\sqrt{\frac{\alpha}{g_{th}}}, \tag{8}$$

which is higher than the single-stage value by a factor of 1.06. This zero-bias detectivity enhancement will continue to increase as the number of stages is increased. For a large number of stages, the equation for the detectivity will be similar to Eq. 8, but with the numerical prefactor approaching the value of $8^{-1/2}$ as the number of stages is increased. This corresponds to an upper limit improvement of 1.1 times higher D^* than the single-absorber case.

II.B.5. Comparison of Single-Absorber and ICIP in Strong-Signal Limit

Here, we will apply the developed theory to investigate the case of signal-limited detection. This is relevant for certain applications such as optical communication and heterodyne detection, which utilize laser sources. In this limit, it is expected that the best detectors will be those that make the most efficient usage of the incident photons. Thus, we will consider ICIPs that have been designed to achieve an equal photo-collection current in each stage, by varying the absorber thicknesses across the structure. This is referred to as a photocurrent-matched ICIP design. In the strong-signal limit, the photo-collection current G_m is strong enough that $G_m >> \Gamma_m$ in each stage. Thus, the noise comes directly from the fluctuations associated with signal current flow itself. Since we dealing with a photocurrent-matched design, no compensating injection current across any of the stages is required for realizing current-matching, so the condition of $G_m >> R_m$ holds as well. Here, we shall evaluate the detector sensitivity directly from the signal-to-noise ratios of the different designs. The signal current is given by:

$$i_s = e\eta_{ext}\Phi_o A\ , \tag{9}$$

where η_{ext} is the external quantum efficiency and Φ_o is the incident photon flux. For the situation where G_m is much greater than Γ_m and R_m, Eq. 6 reduces to:

$$s_o = 2e^2 A\sum_{m=1}^{N_s}\beta_m^2 G_m \tag{10}$$

In the high signal regime, the overall voltage will be applied equally to each stage, so $\beta_m = 1/N_s$. The overall squared noise current can then be written:

$$i_n^2 = \frac{2e^2 A\eta_{ext}\Phi_o}{N_s}\Delta f \tag{11}$$

where we have utilized the condition: $G_1 = G_2 = ... = G_{N_s} = \eta_{ext}\Phi_o$ for photocurrent-matched detectors. The overall signal to noise ratio (SNR) for an arbitrary number of stages is then given by:

$$SNR = \sqrt{\frac{\eta_{part}\Phi_o A}{2\Delta f}}\ , \tag{12}$$

where we have defined the quantity $\eta_{part} = N_s\eta_{ext}$ as the *particle conversion efficiency*. This metric indicates how efficient the device utilizes the incident photons. We see that Eq. 12 reduces to the standard expression for a single-absorber photovoltaic detector in the case of N_s = 1:

$$SNR = \sqrt{\frac{\eta_{ext}\Phi_o A}{2\Delta f}}. \quad (13)$$

It can be seen that when the incoming optical signal strong enough that the signal current is much greater than the dark current, there is no longer a design tradeoff between signal and noise. Thus, the design goal is simply to achieve as large a particle conversion efficiency as possible. If the absorber material has good extraction properties, such that η_{ext} can be very high for a single-absorber detector, there is limited room for improving the particle conversion efficiency by utilizing additional stages. However, when the photocarrier extraction properties of the absorber are poor, as indicated by the absorber product αL_n, adding additional stages can greatly enhance η_{part}. Thus, as with the earlier cases discussed above, the multiple-stage approach will be useful when the product αL_n of the absorber material is relatively low.

II.C. Discussion

ICIPs utilize the unique features of the 6.1 Å family of semiconductors to construct multiple-stage interband PV detectors. The key difference between these detectors and conventional single-absorber PV detectors is that individual electrons must be photo-excited several times in order to pass between the device contacts. The partitioning of the optical signal into the various stages limits the amount of signal current in the device. However, the fact that the electrons must undergo a separate interband transition in each stage also leads to a reduced detector noise. The reduction in noise for ICIPs with additional stages is similar to the reduction in uncertainty associated with adding trials to an experimental measurement. The trade of lower signal for less noise is a potentially useful trade in situations where the absorber material's diffusion length is less than the absorption depth. Multiple-stage devices can employ short absorbers throughout the structure to ensure an efficient usage of the incident photons. When the absorber material has a fairly low value of αL_n, many of the photons that drive the photo-collection current in the optically deeper stages of a multiple-stage detector would be wasted in single-absorber detectors because they would recombine before producing signal.

By applying the theory to evaluate how ICIPs may be able to improve the signal-to-noise ratio of photocurrent-matched detectors, we found that in the strong-signal limit, the signal-to-noise ratio of both single- and multiple-stage detectors directly depended on the particle conversion efficiency of photons to electrons. ICIPs will be beneficial when recombination limits the collection in single-absorber detectors, since in multiple-stage architectures, shorter absorbers can be utilized to improve the collection efficiency. This conclusion is in line with earlier assertions that ICIPs are most useful in situations where full photo-carrier extraction would be difficult with a single absorber detector. Combined with previous results, we can generally say that ICIPs offer the most benefit in situations where a particular material has been judged as a good candidate for an infrared detector based on the absorption and carrier lifetime properties, but is limited by poor extraction of photo-generated carriers. This situation is typically encountered for detectors operating at high temperatures, where the diffusion length is significantly reduced. Recent demonstrations of ICIPs operating at high temperatures (>400 K) [22-24] is a strong validation of the advantages of ICIPs.

III. Experimental Investigations of ICIPs

ICIP structures were designed and grown on nominally undoped p-type GaSb substrates using a Vecco Gen II molecular beam epitaxy (MBE) machine. The five wafers were used to fabricate mid-wavelength (MW) IR detectors are denoted as C1a, C1b, C2, C3, and C15. The number in each of the sample names denotes the number of stages in the device. The basic stage design and choice of SL period was the same for each of the wafers. The primary design difference between the five wafers was in the choice of the number of stages and absorber thickness. Wafers C1a and C1b were both single-stage devices, with total absorber thicknesses of 274 SL periods (~1.32 μm) and 484 SL periods (~2.32 μm), respectively. Wafers C2 and C3 were multiple-stage devices, where the absorber thicknesses were varied across the structure in order to achieve a rough matching of the photocarrier generation rate in each stage. In these samples the optically deeper stages were made thicker, since light attenuation in the shallower stages causes fewer photons to be incident on these stages. The absorbers in the two stages in wafer C2 had 126 (~605 nm) and 148 (~710 nm) periods respectively. The absorbers in three stages in wafer C3 had 132 (~634 nm), 157 (~754 nm), and 195 periods (~936 nm), respectively. Wafer C15 was designed to have 15 identical stages. The absorbers in this structure were fairly short, consisting of 33 SL periods (~158 nm). Note that the total absorption thicknesses of C2 was equal to the absorber thickness of C1a, and that the total absorption thicknesses of C1b, C3, and C15 are also equivalent. Square mesa devices were processed from these ICIP wafers. The photodiodes were fabricated using standard UV lithography with a mask set composed of devices with edge sizes ranging from 200 μm to 1.0 mm. More details about wafers and relevant device fabrication are provided in Ref. 3.

Dark current, photocurrent, quantum efficiency spectra of these devices were obtained at various temperatures from about 80 to 350 K. The cutoff wavelength varied from about 4.3 μm at 78 K to 5.1 μm at 300 K. The advantages offered by the multiple-stage architecture were clearly validated by comparing the temperature-dependence of the photocurrent. Figure 6 shows the temperature-dependence of the detector response under a 500 K blackbody, which is the photocurrent that flows under that illumination divided by the incident power. For both samples C1a and C1b, an increase in photocurrent is observed at low temperatures, and after peaking shows a sharp decrease at high device temperatures. For C1a, the decrease in photocurrent begins around 200 K, while for C1b it begins around 250 K. This is consistent with the observation of the high temperature $(R_oA)^{-1}$ roll-over occurring at a lower temperature for C1a than C1b. The devices from samples C2 and C3 show a monotonic increase in photocurrent with temperature up to about 325 K until the signal begins to drop. The devices from sample C15 show a constant rise in signal with increasing temperature, which is expected for devices with such short absorber lengths. One possibility for why the photocurrent drops so strongly in the single-stage devices at high temperature is that the light is coming in from opposite the collection point. This is the case if the transport is governed by the dynamics of the minority electrons. More results of deice characterizations and discussion are detailed in Ref. 3.

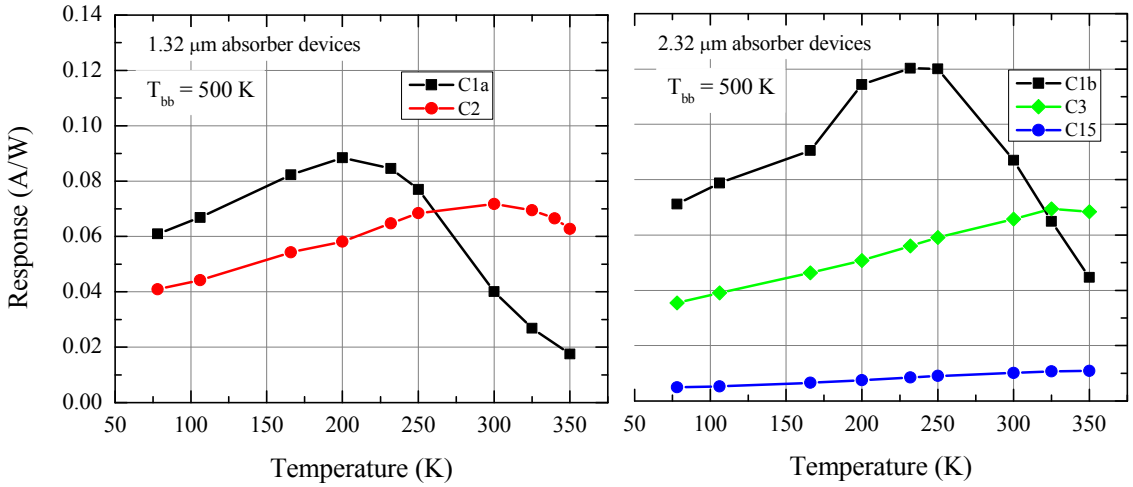

Figure 6. Temperature-dependent response (photocurrent divided by incident power) of MWIR ICIPs under a 500 K blackbody is shown in (a) for samples that had a total absorber thickness of 1.32 and in (b) for samples that had a total absorption thickness. Note that response is the photocurrent that flows in the device divided by the incident power.

IV. Further Remarks

The characteristics of ICIPs that have investigated and demonstrated in this project have suggested a great potential of these devices to achieve high performance needed for many applications. The flexibility of ICIP architecture coupled with quantum engineering should provide considerable improvements in several aspects of device performance, which merits further development. These results from our studies are encouraging. Nevertheless, because ICIPs are new and relatively complicated, with many interfaces and strained thin layers, their growth by MBE is challenging. Thus, ICIP devices are still in their infancy and aspects of the underlying physics are not yet well understood. Extensive research toward improving the material quality and deepening our understanding of their operation is therefore needed to fulfill their promise for practical applications. Furthermore, extension to other aspects is promising based on unique features of ICIPs. For example, in contrast to the continuous absorber design in a conventional photodiode, ICIPs employ a discrete absorber architecture (similar to QWIPs) where electrons move quickly across a short distance in an individual absorber and are capable of *high-speed* operation without compromising absorption quantum efficiency, while still suppressing noise and maintaining reasonably-high detectivity. These high-speed ICIPs will be desirable particularly with the increased use of lasers for applications, such as free-space communication and heterodyne detection. With the development and availability of high-performance room-temperature quantum cascade and IC lasers in the mid-IR spectrum, one can expect growing demands and applications for high-speed detectors that operate at thermoelectric cooler temperatures with high performance. Currently, only limited QWIPs that typically operated in cryogenic temperatures are available in high-speed operation.

The project was originally planned for three years. Due to the budget cut with the sequestration in 2013, the project was terminated earlier. Hopefully, the relevant research will be restored in the future.

Acknowledgements

The work was carried out in collaboration with Robert T. Hinkey, Lu Li, Hossein Lotfi, Hao Ye, Joel C. Keay, Tetsuya D. Mishima, Michael B. Santos, and Matthew B. Johnson at the University of Oklahoma (OU). Research at OU was supported in part by AFOSR (award No. FA9550-12-1-0260), and by C-SPIN, the Oklahoma/Arkansas MRSEC (DMR-0520550).

References

1. R.T. Hinkey and R. Q. Yang, "Dark current modeling of interband cascade infrared photodetectors", at 11th International Conference on Mid-Infrared Optoelectronics Materials and Devices, Chicago, Sept. 4-8, 2012
2. R. T. Hinkey and R. Q. Yang, "Theory of Multiple-Stage Interband Photovoltaic Devices and Ultimate Performance Limit Comparison of Multiple-Stage and Single-Stage Interband Infrared Detectors", J. Appl. Phys. **114**, 104506 (2013).
3. R. T. Hinkey, L. Li, H. Ye, H. Lotfi, R. Q. Yang, L. Lei, J. C. Keay, M. B. Johnson, and M. B. Santos, "Interband cascade infrared photodetectors with InAs/GaSb superlattice absorbers", Paper 8868-3 at Infrared Sensors, Devices, and Applications III, SPIE Optics + Photonics 2013, San Diego, CA, 25 - 29 August 2013; Proc. SPIE **8868**, paper 886805 (2013).
4. R. T. Hinkey and R. Q. Yang, "Comparison of ultimate limits of interband cascade infrared photodetectors and single-absorber detectors", Paper 8868-2 at Infrared Sensors, Devices, and Applications III, SPIE Optics + Photonics 2013, San Diego, CA, 25 - 29 August 2013; in Proc. SPIE **8868**, paper 886804 (2013).
5. R. T. Hinkey, "Multiple-Stage Interband Cascade Photovoltaic Devices using 6.1 Å Semiconductor Materials", Ph.D. dissertation, University of Oklahoma (2013).
6. R. Q. Yang, "Infrared laser based on intersubband transitions in quantum wells," at *7th Inter. Conf. on Superlattices, Microstructures and Microdevices*, Banff, Canada, Aug. 22-26, 1994; Superlattices and Microstructures **17**(1), 77-83 (1995).
7. Rui Q. Yang, "Novel Concepts and Structures for Infrared Lasers", Chap. 2, in *Long Wavelength Infrared Emitters Based on Quantum Wells and Superlattices*, edited by M. Helm (Gordon & Breach Pub., Singapore, 2000).
8. Rui Q. Yang, "Interband Cascade (IC) Lasers", Chap. 12, in *Semiconductor lasers: fundamentals and applications*, edited by A. Baranov and E. Tournie (Woodhead Publishing Limited, Cambridge, UK, 2013.
9. J.V. Li, R.Q. Yang, C.J. Hill, and S.L. Chuang, "Interband cascade detectors with room temperature photovoltaic operation," Appl. Phys. Lett. **86**, 101102 (2005).
10. R. Q. Yang, Z. Tian, Z. Cai, J. F. Klem, M. B. Johnson, and H. C. Liu, "Interband cascade infrared photodetectors with superlattice absorbers", J. Appl. Phys. **107**, No. 5, 054514 (2010).
11. Z. Tian, R. T. Hinkey, R. Q. Yang, D. Lubyshev, Y. Qiu, J. M. Fastenau, W. K. Liu, M. B. Johnson, "Interband Cascade Infrared Photodetectors with enhanced electron barriers and *p*-type superlattice absorbers", J. Appl. Phys. **111**, 024510 (2012).
12. D. Z.-Y. Ting, C. J. Hill, A. Soibel, S. A. Keo, J. M. Mumolo, J. Nguyen, and S. D. Gunapala, "A high-performance long wavelength superlattice complementary barrier infrared detector," *Appl. Phys. Lett*. **95**, 023508 (2009).
13. J. Piotrowski, and A. Rogalski, "Comment on: 'Temperature limits on infrared detectivities of InAs/InGaSb superlattices and bulk HgCdTe," J. Appl. Phys. **80**, 2542-2544 (1996).
14. J. Piotrowski, and W. Gawron, "Ultimate performance of infrared photodetectors and figure of merit of detector material," Infrared Phys. Tech. **38**, 63-68 (1997).
15. C. Donolato, "A reciprocity theorem for charge collection," Appl. Phys. Lett. **46**, 270-272 (1985).

16. M.A. Green, “Generalized relationship between dark carrier distribution and photocarrier collection in solar cells,” J. Appl. Phys. **81**, 268-271 (1997).
17. M.A. Green, “Do built-in fields improve solar cell performance?” Prog. Photovolt. Res. Appl. **17**, 57-66 (2009).
18. R. Q. Yang, Z. Tian, J. F. Klem, T. D. Mishima, M. B. Santos, and M. B. Johnson, “Interband cascade photovoltaic devices”, Appl. Phys. Lett. **96**, No. 6, 063504 (2010).
19. A. Delga, M. Carras, L. Doyennette, V. Trinité, A. Nedelcu, and V. Berger, “Predictive circuit model for noise in quantum cascade detectors,” Appl. Phys. Lett. **99**, 252106 (2011).
20. A. Delga, M. Carras, V. Trinité, V. Guériaux, L. Doyennette, A. Nedelcu, H. Schneider, and V. Berger, “Master equation approach of classical noise in intersubband detectors,” Phys. Rev. B **85**, 245414 (2012).
21. A. Delga, L. Doyennette, M. Carras, V. Trinité, and P. Bois, “Johnson and shot noise in intersubband detectors,” Appl. Phys. Lett. **102**, 163507 (2013).
22. N. Gautam, S. Myers, A.V. Barve, B. Klein, E.P. Smith, D.R. Rhiger, L.R. Dawson, and S. Krishna, “High operating temperature interband cascade midwave infrared detector based on type-II InAs/GaSb strained layer superlattice,” Appl. Phys. Lett. **101**, 021106 (2012).
23. Z.-B. Tian, T. Schuler-Sandy, and S. Krishna, “Electron barrier study of mid-wave infrared interband cascade Photodetectors,” Appl. Phys. Lett. **103**, 083501 (2013).
24. R.T. Hinkey, H. Lotfi, L. Lu, R.Q. Yang, J.F. Klem, J.C. Keay, and M.B. Johnson, “Interband Cascade Thermophotovoltaic Devices with Type-II Superlattice Absorbers of ~0.4 eV Bandgap,” The 39th IEEE Photovoltaic Specialists Conference, Tampa, FL, June 16-21, (2013).